



Implications of urbanization on the seasonal dynamics and long-term trends in the thermal climate of a city in the Himalayan foothills of India

Gayatri Singh¹ · Piyush Kumar Ojha¹ · Shivam Kumar Sharma¹ · Priyanka Kumari¹ · Alok Kumar Pandey² · Amit Kumar Mishra¹ · Krishan Kumar¹

Accepted: 28 April 2024

© The Author(s), under exclusive licence to Springer Nature Switzerland AG 2024

Abstract

This study examines the seasonal and long-term variations in land surface temperature over Dehradun, a rapidly expanding city in the Himalayan region of India. MODIS (Terra and Aqua) satellite data from 2000 to 2019 were utilized to assess (i) seasonal variations in surface urban heat island intensity (SUHII) and (ii) trends in land surface temperature (LST). Positive SUHII was observed over Dehradun throughout the year. However, the magnitude of SUHII varies both diurnally and seasonally, with greater intensity during daytime and the rainy season. Furthermore, our analysis reveals that spatio-temporal variations in LST over Dehradun are significantly influenced by land use-land cover (LULC) variables and elevation. Specifically, open and dense forest areas exert a negative influence, while urban built-up areas have a positive impact on LST. We observed that areas in Dehradun and its surrounding regions that underwent a transition in LULC from agriculture/open forest to urban built-up categories experienced the most significant increase in LST. This rise occurred despite a general warming trend observed in night-time LST across the entire study region, possibly due to global warming. Finally, our study demonstrates an increasing trend in annual cooling degree days, the number of cooling days, and electricity consumption in Dehradun. Therefore, our results suggest that urbanization in Dehradun has resulted in increased warming, which in turn, has steadily contributed to the growth in electricity consumption in the region.

Keywords Urban heat island · Land surface temperature · Cooling degree days · Dehradun · Himalayan

Introduction

Through landmark societal transitions such as agriculture, urbanization, and industrialization, humans have profoundly impacted various systems and subsystems on Earth, posing several environmental challenges. In the present-day context, the increase in the worldwide average surface temperature compared to the pre-industrial period (i.e., global warming) is one of the key challenges faced by human society (Hawkins et al. 2017; Schurer et al. 2017). Although global warming is mostly attributed to the unprecedented raise in the

concentrations of greenhouse gases caused by the surge in anthropogenic activities over the last two centuries (Hansen and Sato 2004), the land use-land cover (LULC) change brought about by urbanization is also known to influence the local thermal climate of a place (Oke 2010).

Thus, if a rising temperature trend is observed at a place, it may have a contribution from both global warming caused by greenhouse gases and local warming due to LULC changes associated with urbanization. At the current pace of urbanization, it is expected that approximately 68% of the world's population would reside in urban areas by 2050 (World Urbanization Prospects 2018). A significant part of this increase in urbanization is likely to be concentrated in the low-income and lower-middle-income countries of Asia and Africa. Thus, as urbanization spreads to more areas of the world, the urban footprint on the local and regional thermal climate is also expected to grow.

The land use-land cover (LULC) changes accompanying urbanization involve the transformation of predominantly

✉ Krishan Kumar
krishan_kumar@mail.jnu.ac.in

¹ School of Environmental Sciences, Jawaharlal Nehru University, New Delhi, India

² Lancaster Environment Centre, Lancaster University, Lancaster LA14YQ, UK

vegetated and pervious surfaces into high-density built-up structures with impervious surfaces for industrial, commercial, transportation, and residential activities (Oke 1981; Arnfield 1982; Li et al., 2017; Tabassum et al. 2023). These changes often manifest as the so-called 'urban heat island' (UHI), referring to the phenomenon of urban areas being warmer than the surrounding rural areas (Oke 1982). The formation of UHI adversely impacts the comfort level of residents in urban areas, forcing them to employ devices for space cooling. This puts additional pressure on local energy demand (Akbari et al. 2001; Kumari et al. 2021). Therefore, studying urban climate dynamics is crucial for devising appropriate strategies for a city's energy management.

In this regard, thermal remote sensing techniques (Voogt and Oke 2003) have been widely employed in urban climate studies over the last two decades (e.g., Pu et al. 2006; Buyantuyev et al., 2010; Sobrino et al. 2013; Weng et al. 2014; Chakraborty et al. 2020; Morshed et al. 2022; Dutta et al., 2022; Kimothi et al. 2023; Chetty 2023) due to their definite advantage in terms of spatial coverage. These studies generally examine spatio-temporal variations in satellite-derived land surface temperature (LST) to gain insights into the formation of the surface urban heat island (SUHI).

Most of these studies, however, pertain to plain regions of the world, as cities are preferentially located on flat terrain near rivers or coasts (Oke et al. 2017). However, urbanization is not limited to plain regions. Countries such as India, facing immense population pressure, have witnessed unprecedented urbanization even in hilly regions (Singh et al. 2021; Chetty 2022). In the last few years, several studies (Romshoo and Rashid 2014; Dame et al. 2019; Ullah et al. 2019; Habeeb et al. 2019; Joshi 2021; Diksha et al. 2022) have highlighted the adverse impacts of urbanization in the Himalayan region. Studies examining the urban climate in hilly regions, however, are rather sparse. Understanding the changes in the local climate due to urbanization in hilly regions is more complex and challenging due to the additional influence of altitude on land surface temperature.

Estoque and Murayama (2017) showed that SUHI formed in a tropical mountain city in the Philippines, despite the cool climate of the study area. Similarly, Liao et al. (2021) also examined UHI formation over Chongqing city on hilly terrain in China and suggested a method to estimate the UHI index for cities with such terrain. In the Indian context, however, no attempts have been made (i) to examine the thermal climate variations in hilly urban areas by taking into consideration the altitudinal variations, and (ii) to assess the impact of urbanization-induced changes in thermal climate on cooling degree days (a proxy for energy demand for cooling) and electricity consumption in hilly urban areas.

The present study addresses these aspects by studying the seasonal and long-term variations in the thermal climate of Dehradun, the capital city of Uttarakhand state, India,

situated in the Himalayan foothills. It is pertinent to mention that Dehradun has been included in the list of cities chosen for the Indian Government's Smart Cities Mission, recognizing the need for providing a clean and sustainable environment with the application of 'smart' solutions for waste and energy management (<https://smartcities.gov.in/sites/default/files/SmartCityGuidelines.pdf> downloaded on 23-05-2023). Thus, it becomes important to assess the impact of urbanization on Dehradun's thermal climate and examine its implications for the energy demand and consumption of the city.

Data Description and Methodology

Study Area

In the present work, the study area encompasses the Dehradun city municipality and its surrounding areas, covering a total area of 547 km² (Fig. 1). Dehradun is located in the Indian state of Uttarakhand, positioned between 30.26° N and 30.40° N latitudes and 77.98° E and 78.10° E longitudes at an average elevation of 640 m above mean sea level. The city is bounded by the Himalayan ranges towards the north and the Shivaliks towards the south, the river Song to the east, and the river Tons to the west. Topographically, the city has hilly terrain with elevations ranging from 578 to 1041 m above mean sea level. However, considering the entire study area, the elevation range widens further from 483 to 2058 m above mean sea level.

The climate of Dehradun is characterized by hot summers when maximum temperatures may reach up to 40 °C or even higher during peak summer and cold winters when minimum temperatures may drop to 4 °C or even below during peak winter (Sharma et al. 2012). The average annual rainfall over Dehradun is more than 200 cm, the major part of which is received during the summer monsoon season (Sharma et al. 2012). Over the last two decades, Dehradun has witnessed rapid urbanization. The Dehradun metropolitan area's population grew from 0.535 million in 2001 to 0.713 million in 2011, and its current population is estimated to be 0.992 million in 2023 (Dehradun Population n.d.).

Landsat 7 Data

In the present work, the LULC classification of the study area for the year 2000 was conducted based on Landsat 7 imagery dated February 24, 2000. Equipped with a powerful sensor, Enhanced Thematic Mapper Plus (ETM+), this satellite was launched by NASA in 1999 to capture information on Earth's landmasses. At a height of 705 kms, the satellite is positioned in a sun-synchronous orbit, crossing the equator at approximately 10:00 am on a descending orbital node from north to south. The satellite

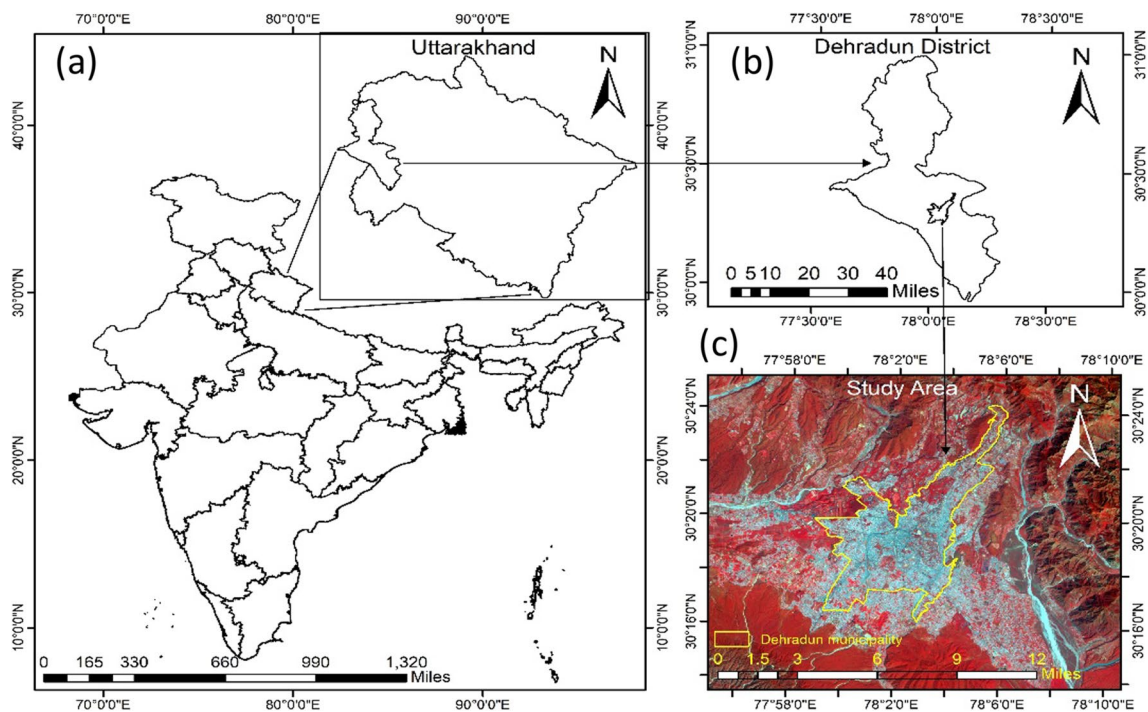


Fig. 1 Location of study area (a) Uttarakhand state; (b) Dehradun district (c) False Color Composite (FCC) map of Dehradun city

has a swath of 185 km with a repeat coverage cycle of 16 days. It captures high-quality data in the visible (bands 1, 2, and 3), infrared (bands 4, 5, and 7) regions of the electromagnetic spectrum at a spatial resolution of 30 m and the thermal (band 6) region at a spatial resolution of 60 m (Goward et al. 2001; Rongali et al. 2018).

Sentinel 2 Data

We utilized a Sentinel 2 image from March 6, 2019, for LULC classification of our study area for the year 2019. Sentinel 2 is made up of two identical satellites, 2A and 2B, in polar orbit, launched by the European Space Agency in June 2015 and March 2017, respectively. Both satellites are placed in a sun-synchronous orbit at an altitude of 786 km and are phased at 180° from each other, providing a revisit time of 5 days with both satellites. The satellite is equipped with a multispectral imaging sensor to capture information about the Earth's surface, with a wide swath of 290 km. The multispectral sensor captures data in 13 bands at spatial resolutions of 10 m (bands 2, 3, 4, 8), 20 m (bands 5, 6, 7, 8A, 11, 12), and 60 m (bands 1, 9, 10) (Phiri et al. 2020).

MODIS LST Data

In the present study, MODIS Terra product (MOD11A2.v061) and MODIS Aqua product (MYD11A2.v061) were used to obtain LST (1 km resolution) over Dehradun city

and the surrounding areas. MOD11A2.v061 and MYD11A2.v061 are 8-days composite average products derived from the MOD11A1 and MYD11A1 daily global products (Wan et al. 2002).

Moderate Resolution Imaging Spectroradiometers (MODIS), mounted on Terra and Aqua satellites, were launched by NASA in December 1999 and May 2002, respectively. Both Terra and Aqua orbit around the Earth in polar sun-synchronous orbits at an altitude of 705 km, with equator crossing times of 10:30 am/pm (Terra) and 1:30 pm/am (Aqua) respectively. The instrument has a wide swath width of 2330 km, enabling it to view every point on Earth's surface in a 1 to 2 days cycle. MODIS captures data in 36 spectral bands ranging from 0.405 to 14.385 μm , at varying spatial resolutions of 250 m (bands 1–2), 500 m (bands 3–7), and 1000 m (bands 8–36) (Vancutsem et al. 2010).

ASTER DEM Data

The Advanced Spaceborne Thermal Emission and Reflection Radiometer (ASTER) is an imaging sensor onboard the Terra satellite, launched by NASA's Earth Observing System in December 1999. ASTER captures high-resolution images of the Earth in 14 different wavelength bands in the visible (bands 1, 2, 3N, and 3B at 15 m spatial resolution), shortwave infrared (bands 4 to 9 at 30 m spatial resolution), and thermal infrared (bands 10 to 14 at 90 m spatial resolution) regions of the electromagnetic spectrum

to obtain useful information on land surface temperature, emissivity, reflectance, and elevation (Hirano et al. 2003; Rana and Suryanarayana 2019). In the present study, the ASTGTMv003 product of ASTER was used to obtain information on elevation (Supplementary Fig. 1).

Land Use Land Cover (LULC) Classification and Change Detection Analysis

For the land use-land cover (LULC) classification, we employed the Maximum Likelihood Classifier (MLC) method of supervised classification. MLC is a very robust method of LULC analysis and has been widely used in several scientific studies across the world (Sun et al. 2013; Ganasri and Dwarakish 2015; Hishe et al. 2021; Mishra et al. 2020; Saha et al. 2021). This classification technique is based on the affinity of the spectral signature of a targeted pixel to the specific class (Otukey and Blaschke 2010). Each pixel's reflectance value is assigned to the class for which it has highest probability of resembling a signature under a probability-based weighting scheme (Strahler 1980; Yuan et al. 2005).

We categorised the study area into seven distinct classes, namely Dense Forest (DFOR), Open Forest (OFOR), Agriculture (AGRI), Fallow Land (FALO), Built-Up (BILT), Water Body (WBOD), and Open Space (OPNS). These classes are very different in terms of their physical properties, (such as- heat capacity, thermal conductivity, emissivity, albedo, moisture content, thermal inertia and sky-view factor) which are known to significantly influence the local thermal climate of a place (Taha 1997; Priyadarsini 2009; Mohajerani et al. 2017; Oke et al. 2017). The accuracy assessment was performed using the stratified random point generation method, which involved generating 50 sample points for each class to obtain a confusion matrix and Kappa statistics for the classified image (Supplementary Tables S1 and S2).

Estimation of Urban Heat Island Intensity (UHII)

For the estimation UHII over the study area, average monthly daytime and nighttime land surface temperatures over the core urban region and four rectangular strips outside Dehradun city (Supplementary Fig. 2) were extracted from the MODIS-Terra and Aqua 8-days composite LST products (MOD11A2.v061 and MYD11A2.v061) at 1 km resolution for the period January 2019 to December 2019. The four strips, named North, South, East, and West, were defined based on their location in relation to the core urban region strip.

For the estimation of UHII, the average LST in each strip outside Dehradun city was subtracted from the average LST over the core urban region of Dehradun city. In this way,

we calculated UHII for the study area. However, since LST is known to be influenced by elevation (Khandelwal et al. 2018), the average elevation of each of these strips was also taken into consideration while analysing our results.

Air Temperature Data and Computation of Cooling Degree Days

In the present study, air temperature data for Dehradun from <https://www.visualcrossing.com/> was utilized to obtain the trend in cooling degree days for Dehradun for the period 2003 to 2022. This dataset provides the air temperature for the location (30°31'N and 78°03'E) in Dehradun. Cooling Degree Days (CDDs) indicate how hot a given day is relative to a base temperature, are a useful measure of the cooling requirements of a city (Christenson et al. 2006; Jiang et al. 2009; Rosa et al. 2015; Borah et al. 2015; Ukey and Rai 2021). In the present study, for the computation of cooling degree days (CDDs) we subtracted the base temperature of 18 °C (Bhatnagar et al. 2018) from the average temperature for those days when the average temperature exceeded the base temperature. For instance, if the average temperature of the day is 30 °C, the CDDs for that day is 12 °C. Adding all the CDDs in a given year gave us the annual magnitude of CDDs. Counting the number of days in a year when the average temperature was greater than the base temperature provided us with the annual frequency of CDDs.

Furthermore, for the computation of pixel-wise trends in cooling degree days for Dehradun, we initially validated the MODIS LST data with air temperature data by considering the LST data of the pixel corresponding to the site for the collection of air temperature data. For the computation of mean LST, the mean of Aqua daytime and night-time LST was calculated. The scatter plot (Fig. 2) between the mean MODIS LST and mean air temperature shows a strong agreement between them with

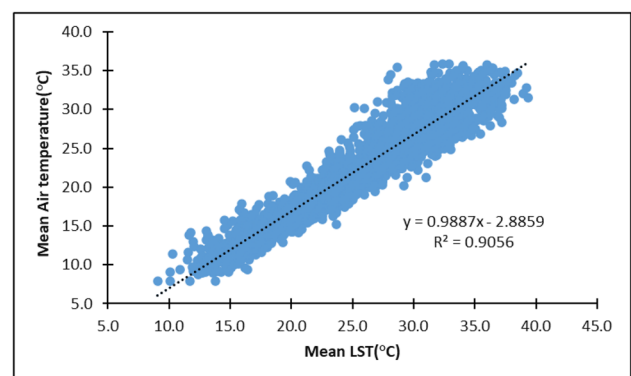


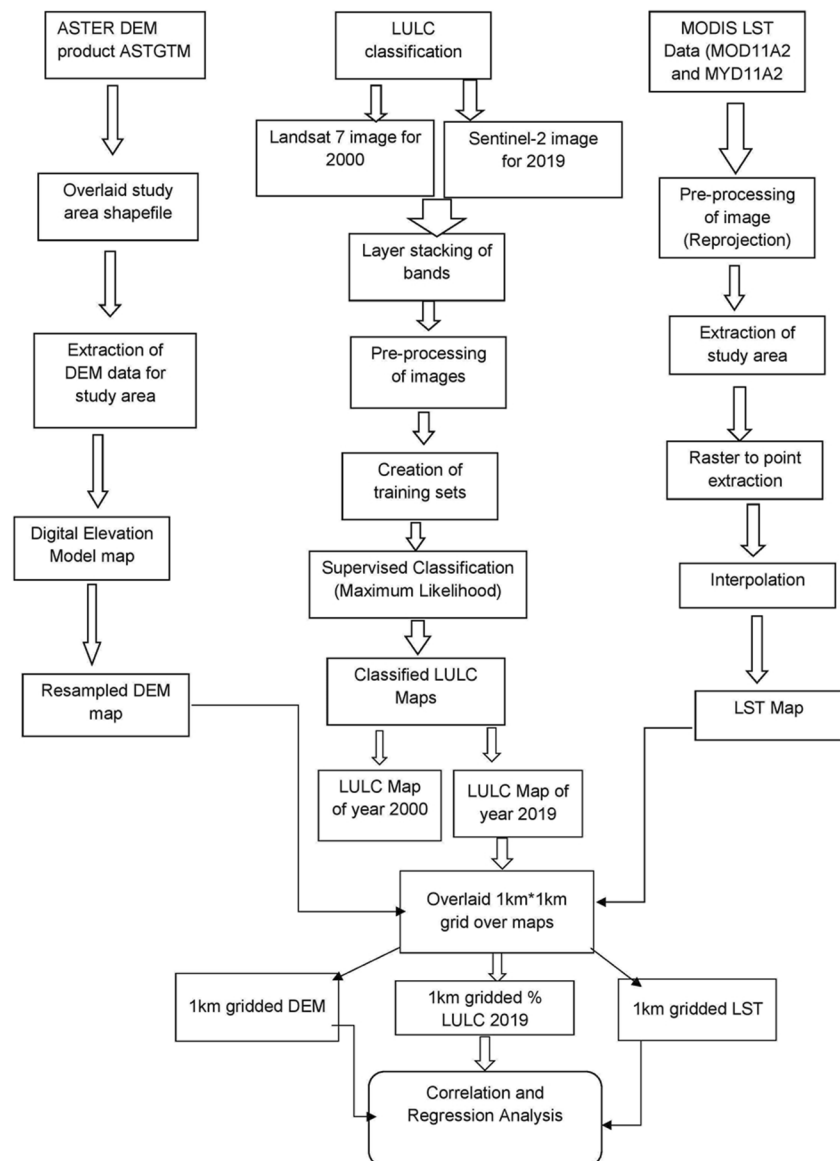
Fig. 2 Scatter plot between mean air temperature and mean LST

an R^2 value of ~ 0.9 , Index of Agreement value ~ 0.97 and Normalized Mean Square Error value ~ 0.0085 . The regression equation of the best-fit line between mean MODIS LST and mean air temperature was then used to derive the mean air temperature pertaining to each MODIS LST pixel. The mean air temperature obtained for each pixel was then used to compute the trend in the annual magnitude and frequency of cooling degree days for each pixel. It is pertinent here to mention that we have assumed that the equation governing linear relationship between average air temperature obtained from weather station and the mean LST of the pixel where the weather station is located, is applicable for all the pixels in the study region. This is one of the limitations in the present

study, as average air temperature data was available from only one weather station in Dehradun.

The flow chart (Fig. 3) given below describes different steps followed in the preparation of DEM, LST and LULC maps used in this study. For LULC classification Landsat-7 and Sentinel-2 images (2000 and 2019) were taken. Layer stacking of bands and pre-processing of image were done and then created training signatures for all the LULC classes. With the help of Supervised classification method (Maximum Likelihood) the LULC map was classified. Further, 1 km*1 km grid was overlaid on DEM, LST and LULC maps and all the gridded data obtained were used in the statistical correlation and regression analysis.

Fig. 3 Flow Chart of the steps involved in the methodology



LULC changes over Dehradun and surrounding areas from 2000 to 2019

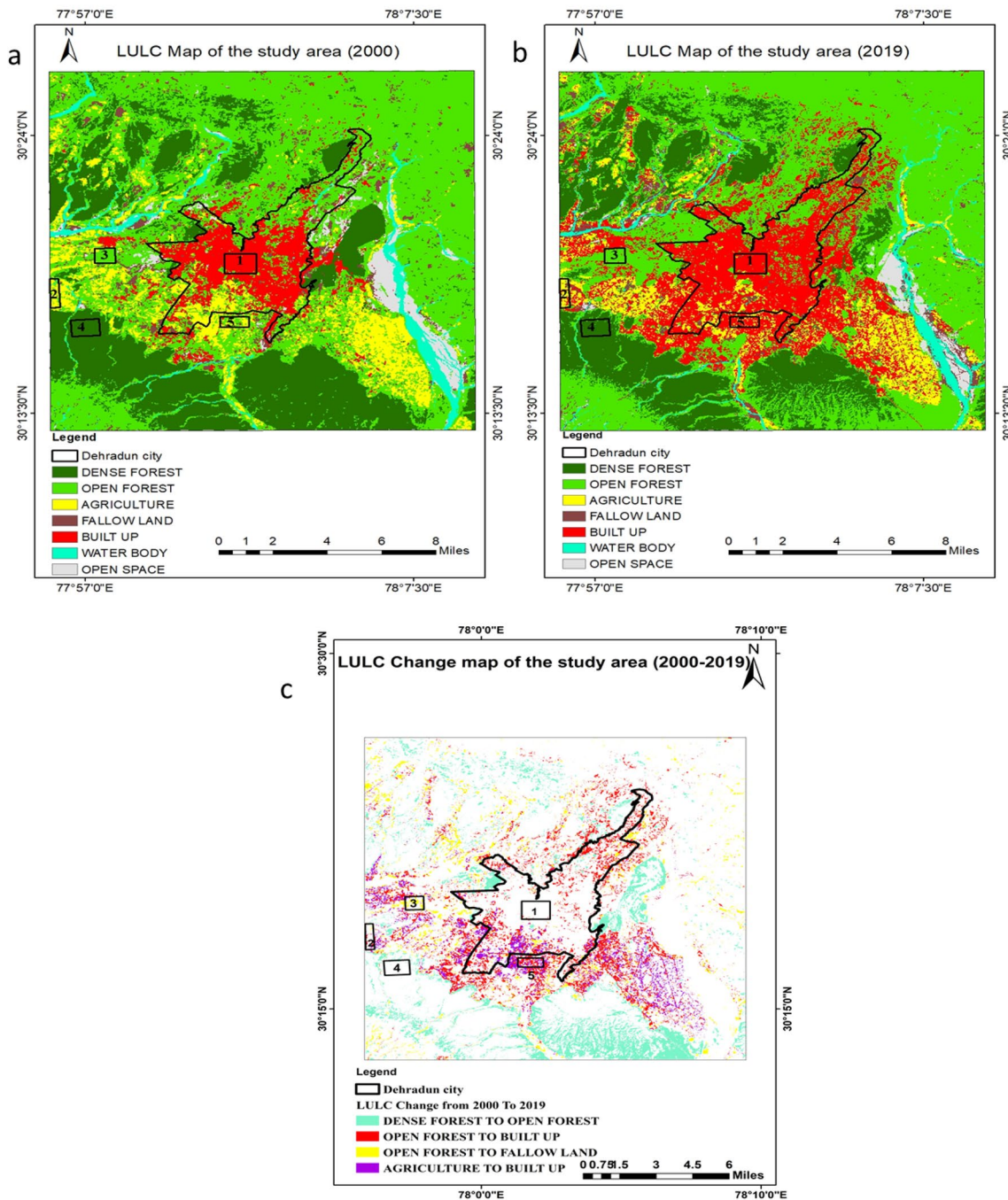


Fig. 4 Land use and land cover distribution over Dehradun city and its surrounding area for the years (a) 2000, (b) 2019, (c) LULC changes from 2000 to 2019. The rectangular boxes shown by numerals 1 to 5 represent typical areas with/without any change in LULC

from 2000 to 2019 as follows: 1-Built-up to built-up,2-Agriculture to agriculture,3-Open forest to open forest,4-Dense forest to dense forest,5-Agriculture/Open forest to built-up

Results and Discussion

Urbanisation and LST Trends Over Dehradun

The state of Uttarakhand in India was carved out of the existing state of Uttar Pradesh in the year 2000, and Dehradun was declared as the capital of this newly formed state. Ever

since then, Dehradun has witnessed rapid urbanization. Figure 4a and b represent the classified images of Dehradun from Landsat-7 and Sentinel-2 for the years 2000 and

2019, respectively. Figure 4c represents the major LULC changes over the study region from 2000 to 2019. Landsat-7 for the LULC analysis in the year 2000 was chosen as it is the open access multispectral data available from NASA. We could not use the Landsat-7 data for 2019 LULC analysis as Scan line corrector (SLC) error has appeared in the Landsat-7 data since 2003 (Landsat-7 data (<https://www.usgs.gov/landsat-missions/landsat-7>), n.d). So, for the LULC analysis for the year 2019, we were left with the option of using Sentinel-2 data or Landsat-8 data. In our study, we preferred Sentinel-2 data because of its better spatial resolution.

A comparative visual examination of the images reveals the growth of the built-up area within the Dehradun city municipality area, both in the northern and southern parts. However, this expansion is not confined to the city boundaries alone. Significant growth in the built-up area is observed in the surrounding regions to the south, south-east, and south-west of the city. With relatively flat terrain and low altitude, these regions are more conducive to the growth of the built-up area. Urban expansion in the surrounding region lying north and north-east of the city has been somewhat limited due to high altitude, though some growth in the built-up area can be seen in these regions also.

Figure 4c shows major classes which have undergone LULC change during the study period, i.e., dense forest to open forest, open forest to built-up, open forest to fallow land and agriculture to built-up are shown with different colours. Other classes which have not witnessed any change or negligible change are shown with white colour for proper discrimination of the LULC change.

Table 1 Typical areas with/without any change in LULC from 2000 to 2019, as represented by different rectangular boxes in Figure

Box Number	LULC class in 2000	LULC class in 2019
1	Built-up	Built-up
2	Agriculture	Agriculture
3	Open forest	Open forest
4	Dense forest	Dense forest
5	Agriculture/Open forest	Built-up

To analyse the impact of urbanization, we examined MODIS LST trends over the study region at places that have not witnessed any LULC change during the last two decades and those that have undergone a transition from agriculture/open forest to built-up areas. These places have been represented by different rectangular boxes in Fig. 4 according to the scheme given in Table 1.

We hypothesized that places which have undergone a change in land use and land cover (LULC) from agriculture/open forest to built-up (e.g., rectangular box 5) during the study period were expected to experience the sharpest rise in land surface temperature (LST) among all classes. This is revealed in Fig. 5(a-d), which shows the spatial distribution of LST trends over the study region. Averaged LST trends at places pertaining to different rectangular boxes (Table 1) are also provided separately in Supplementary Figure S3(a-j).

It is observed that the increasing trend in land surface temperature (LST) over places that have undergone LULC change from agriculture/open forest to built-up is much higher (0.12 to 0.13 °C/yr) for nighttime Aqua and Terra data (Fig. 5a and b and Figure S3i), compared to LST trends ranging from 0.03 to 0.05 °C/yr over places that have not witnessed any LULC change from 2000 to 2019 (Fig. 5a and b and Supplementary Figure S3-a, c, e, g). The relatively smaller positive LST trends during nighttime at places that have not witnessed any change in LULC during the last two decades suggest that there is a general warming in the study region, possibly occurring due to global warming. However, at places that have witnessed urbanization due to a change in LULC from agriculture/open forest to built-up, the impact of urbanization adds to this general warming trend.

During the daytime, land surface temperature (LST) trends over places that have undergone LULC change from agriculture/open forest to built-up show positive slope coefficients (~0.02 to 0.05 °C/yr) for Terra and Aqua data, respectively (Fig. 5c and d and Supplementary Figure S3j), compared to almost zero or negative slope coefficients over places that have not witnessed any LULC change from 2000 to 2019 (Fig. 5c and d and Supplementary Figure S3-b, d, f, h). The comparatively reduced positive LST trend for places which have undergone a change in LULC and negative LST trends for places that have not witnessed any LULC change during the daytime are possibly due to an increase in solar dimming over the study region because of an increase in cloud cover. MERRA-2 derived datasets, which assimilate observations from various satellites (e.g., MODIS, MISR), reveal an increasing trend in cloud cover over the Dehradun region during the last two decades (Supplementary Figure S4).

Cox et al. (2020) have suggested that there exists a diurnal asymmetry in global warming due to the increase in cloud cover over the humid and wetter regions of the world. They have shown that nighttime surface temperatures increase

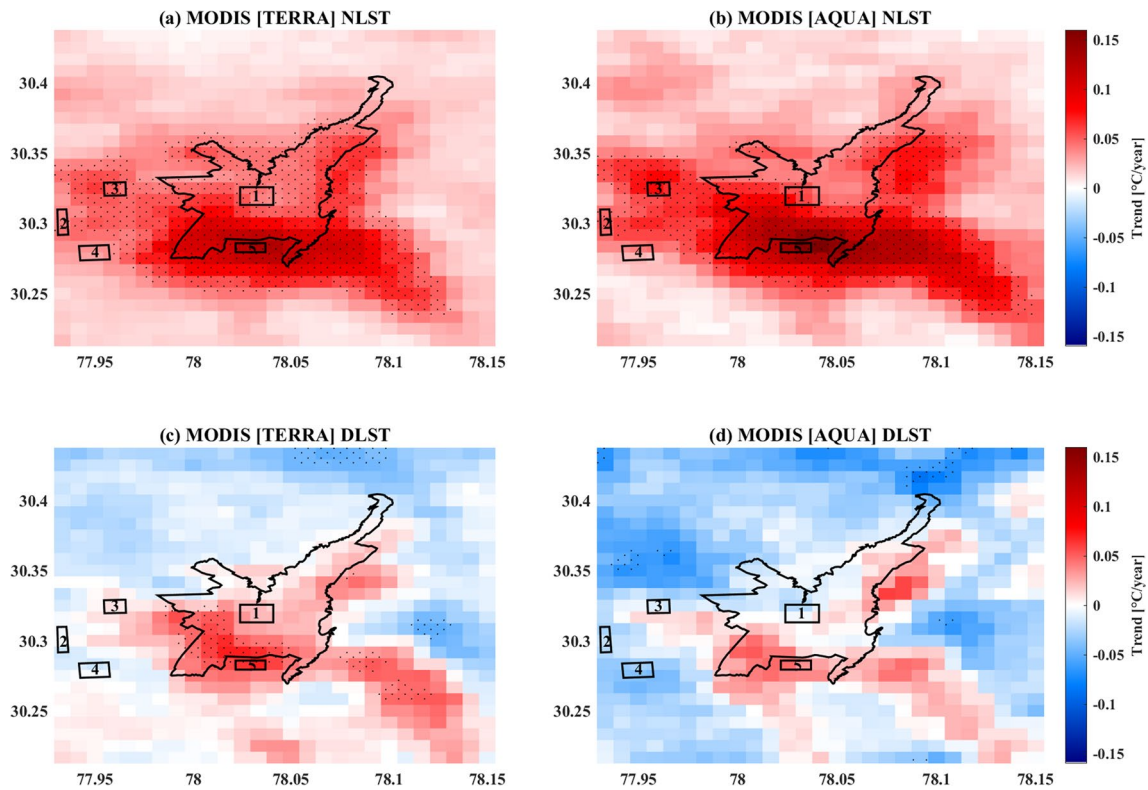


Fig. 5 (a-d) LST trends over Dehradun city and the surrounding areas showing enhanced warming at places which have undergone urbanization during the period 2000 to 2019

more than the corresponding daytime temperatures due to increased cloud cover under global warming. During the daytime, these clouds predominantly attenuate the incoming shortwave solar radiation, thereby inducing surface dimming and cooling (Rieck et al. 2014; Pyrgou et al. 2019). On the contrary, during the nighttime, the clouds absorb the outgoing longwave radiation and reradiate it back towards the surface, thereby causing raise in surface temperature (Pyrgou et al. 2019).

Being in the Terai belt of India, Dehradun has a somewhat humid and wet climate, with significant rainfall in almost all months of the year (Sharma et al. 2012). Therefore, the increasing trend in annual cloud cover over Dehradun (Supplementary Figure S4) seems to be the most plausible reason for the observed land surface temperature (LST) trends during day and nighttime. Moreover, despite the diminishing effect of increased cloud cover during the daytime, the regions that have undergone urbanization (i.e., a change in land use and land cover from agriculture/open forest to urban built-up) show a positive trend in LST, though weak compared to that in the nighttime. Finally, to summarize, the increasing trend in cloud cover over the

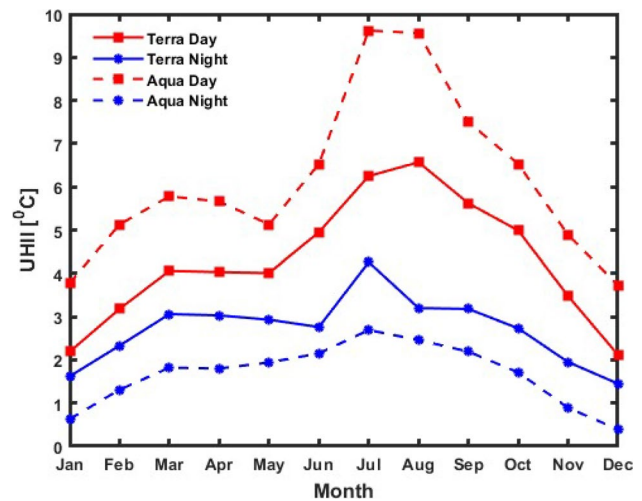


Fig. 6 Day and Night SUHII over the study area using MODIS Terra and Aqua observations

study region seems to counteract the warming during the day while playing a supportive role in warming during the night.

Urban Heat Island Intensity over Dehradun and its Seasonal and Diurnal Dynamics

As mentioned in the methodology section, we computed monthly surface urban heat island intensity for each of the four strips (i.e., north, south, east, and west) surrounding the urban core using daytime and nighttime MODIS LST data from Terra and Aqua.

The climatology of the seasonal variations in surface urban heat island intensity (SUHII) obtained by averaging the data for the entire study duration is presented in Fig. 6. The plots in Fig. 6 reveal several interesting features of SUHI formation over Dehradun.

It is observed that the urban core remains warmer than the surrounding rural areas during both day ($\sim 2\text{--}6\text{ }^{\circ}\text{C}$ for Terra and $\sim 4\text{--}9\text{ }^{\circ}\text{C}$ for Aqua) and night ($\sim 1.5\text{--}3.5\text{ }^{\circ}\text{C}$ for Terra and $\sim 0.5\text{--}2\text{ }^{\circ}\text{C}$ for Aqua) in all seasons. In other words, positive SUHII is observed throughout the year over Dehradun. This observation is at variance from several Indian cities that show negative SUHII (i.e., cool island formation) during the daytime in some seasons (Pandey et al. 2012, 2014; Shastri et al. 2017). This is plausible because the surrounding strips of Dehradun are predominantly covered with vegetation (open forest/dense forest) throughout the year. A comparatively small fraction of the surrounding strips is cropland which may undergo seasonal variation in LULC from agriculture to fallow land depending on the crop cycle.

In the context of Delhi, Pandey et al. (2014) have shown that daytime SUHII is positive (i.e., surface heat island formation) in the months of February–March when Delhi surrounding regions are adorned with crop vegetation. They attribute this behaviour to the comparatively higher thermal inertia of vegetation. Thus, if the surrounding regions of Dehradun are predominantly adorned with vegetation (open/dense forest) throughout the year, their heating up during the daytime is comparatively slower, and daytime SUHII is always positive.

Another feature of SUHI formation over Dehradun is that the magnitude of SUHII is generally greater in the daytime than that during the nighttime (Fig. 6). Generally, the vegetated area tends to heat up slowly during the daytime because of latent heat loss through evapotranspiration (Gu et al. 2021) as compared to urban built-up. Moreover, the thermal inertia of vegetation being greater than the urban building materials (Carnahan and Larson 1990; Sobrino and Kharraz 1999), it is expected that surrounding areas of Dehradun would heat up slower than the urban built-up area during the daytime, leading to high values of SUHII. Also, the emission of anthropogenic heat in the urban core is expected to be greater during the daytime as compared to nighttime,

which further strengthens the daytime SUHII. Further, it may be observed that the daytime SUHII is maximum at Aqua overpass time (i.e., 1.30 pm) since heating of the urban core relative to surrounding strips is maximum at this time.

During the nighttime, the greater thermal inertia of the vegetated surrounding regions favours slower cooling compared to the urban-core built-up area. This tendency tends to offset the relatively greater efficiency of radiative cooling over the surrounding regions during nighttime because of better sky-view factors there. Thus, the nighttime SUHII is somewhat diminished compared to the daytime SUHII. Furthermore, it may be observed that the nighttime SUHII is minimum at the Aqua overpass time (i.e., 1.30 am) since the impact of lower thermal inertia of the urban core relative to the surrounding strips would be more pronounced at this time.

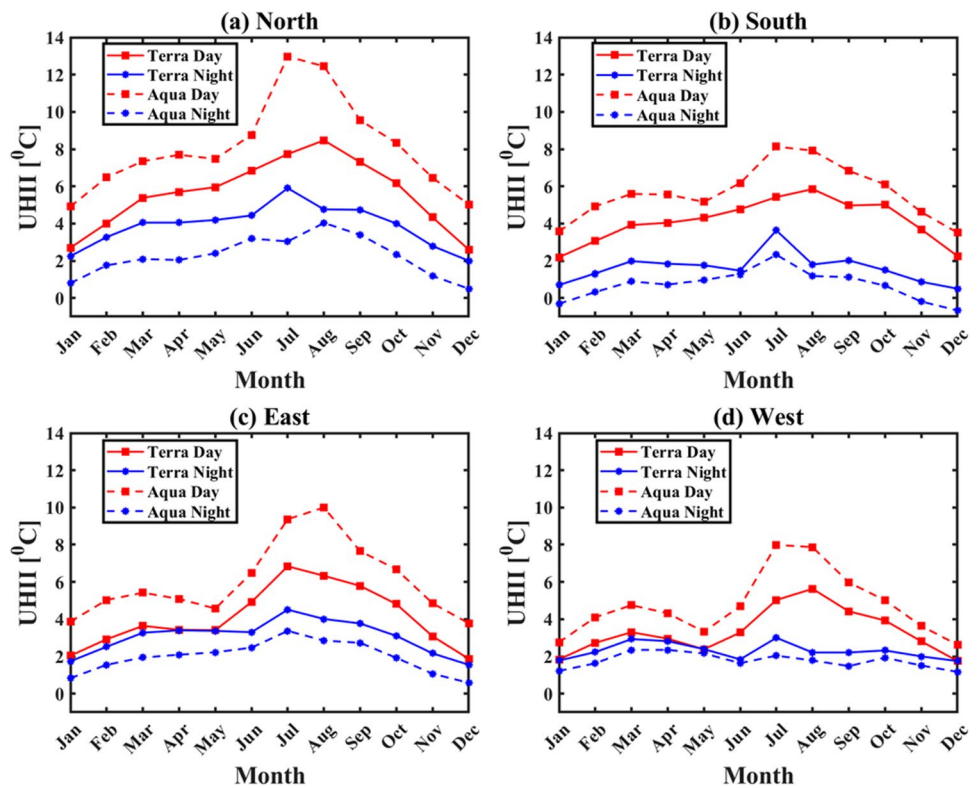
Another feature of SUHI formation over Dehradun is the seasonal variation in the magnitude of SUHII (Fig. 6). It is observed that SUHII over Dehradun is generally minimum during the winter months of December and January ($< 2\text{ }^{\circ}\text{C}$), while it reaches its peak values during the monsoon months, i.e., July and August ($> 6\text{ }^{\circ}\text{C}$). The climatology of rainfall over Dehradun (Sharma et al., 2012) reveals that the months of November and December receive the least rainfall while the monsoon months, i.e., July and August, receive the maximum rainfall.

This pattern suggests that the soil moisture over the study region is expected to be less during the winter months and high during the monsoon months. Since the degree of soil moisture directly influences the thermal inertia of soil, i.e., dry soils have low thermal inertia and wet soils have high thermal inertia (Lu et al. 2009), we infer that the thermal inertia of the surrounding strips of Dehradun is maximum during the monsoon months and minimum during the winter months. Thus, the thermal inertia differential between the vegetated surrounding strips and the built-up urban core is expected to be the maximum during the monsoon months. Therefore, the surrounding strips heat up/cool down much slower during the monsoon months, leading to greater values of SUHII in these months. In contrast, the thermal inertia differential between the vegetated surrounding strips and the urban core is minimum during the winters, which leads to lower values of SUHII during these months.

Impact of Elevation on SUHII

As can be seen from Supplementary Figure S2, the surrounding strips to the north (average elevation 1185 m) and east (average elevation 923 m) of Dehradun are at much higher elevations compared to the urban core of Dehradun city (average elevation 660 m). The strips to the south (average elevation 664 m) and west (average elevation 669 m) of the core region are at comparable elevations.

Fig. 7 SUHII with reference to strips located (a) north, (b) south, (c) east and (d) west, of the urban core



To examine the impact of elevation on SUHII, we computed the SUHII with reference to each of the four surrounding strips (i.e., north, south, east, and west), which is shown in Fig. 7. It is seen that the SUHII of the surrounding strips lying north and east of Dehradun is significantly higher than that of the strips lying south and west both during the daytime and nighttime. The scatter plots between elevation and daytime LST over the study region (Fig. 8 and Supplementary figure S5) show a negative association between them, i.e., LST decreases as the elevation increases. Thus, LST of places located at higher elevations is lower than those located at lower elevations. Therefore, daytime SUHII of the surrounding strips located north and east is higher as compared to the strips lying south and west.

During the nighttime, however, the situation is not as straightforward. The scatter plots between elevation and nighttime LST over the study region (Fig. 9 and Supplementary figure S6) show that LST first increases with elevation up to about 1000 m, and thereafter LST decreases with elevation. It may also be noted that this kind of behaviour is not observed in the monsoon months (July to September) when the sky is cloudy, and nighttime cooling is much diminished. This suggests that a temperature inversion layer forms over Dehradun during the nighttime for a major part of the year (i.e., except the monsoon months).

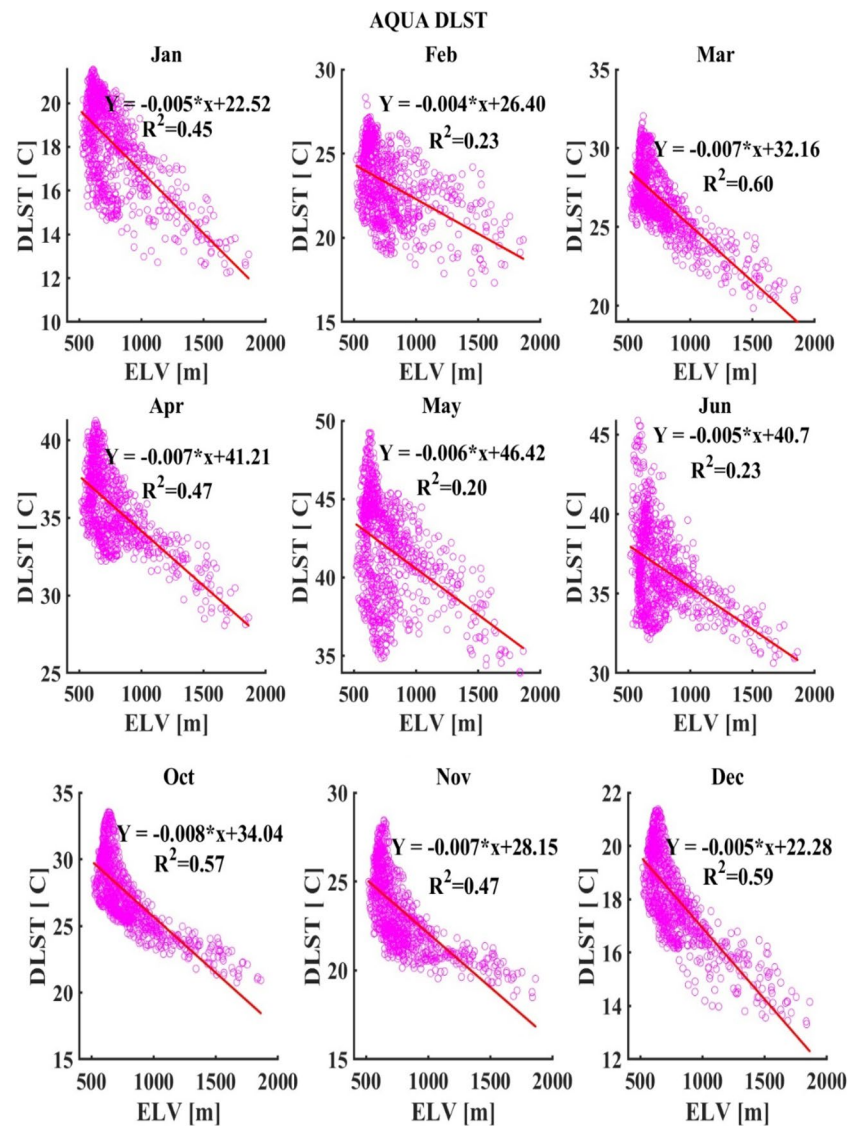
This temperature inversion layer is more pronounced during the winters when nighttime cooling dominates the daytime heating. Such temperature inversions generally

form over a valley because the slopes get cooled during the nighttime, creating downslope or katabatic wind flow which allows the cold air to settle at lower elevations, leading to the formation of a temperature inversion (Ball 1956; Papadopoulos and Helmis 1999; Vihma et al. 2011). Above this inversion layer, LST decreases with elevation as it does during the daytime. Thus, the nighttime SUHII of the surrounding strips lying north and east of Dehradun at average altitude of more than 900 m is also slightly higher than the SUHII of the strips lying south and west of Dehradun.

Association of LST with LULC and Elevation

To gain a deeper insight into the dependence of LST on LULC and elevation, we overlaid a grid over the study region with a grid cell size of 1 km \times 1 km corresponding to MODIS LST data and computed percentage LULC and average elevation for each grid cell to perform correlation and regression analysis. Table 2 presents the correlation of daytime and nighttime LST with percentage LULC and elevation over the study region for March 2019. It is observed that daytime LST (DLST) has a significant positive correlation with Built-up (BILT), Agriculture (AGRI), and Fallow land (FALO), while it has a significant negative correlation with Elevation (ELEV), Dense forest (DFOR), and Open forest (OFOR). These results are expected since agricultural land, fallow land, and built-up areas would heat

Fig. 8 Scatter plot between Aqua Day LST and Elevation



up faster than open and dense forests as their thermal inertia is comparatively lower. It may be noted that the strongest negative association is seen with ELEV while the strongest positive association is seen with BILT.

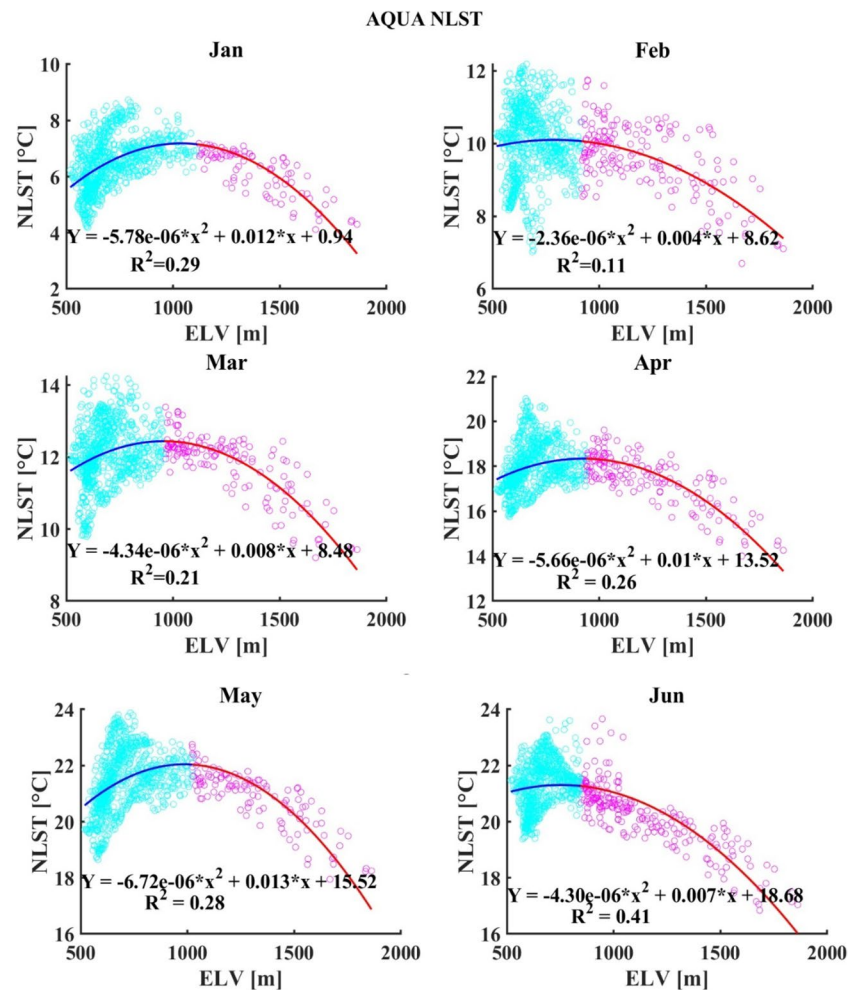
Nighttime LST (NLST) shows a significant positive correlation with DFOR and a significant negative correlation with ELEV, AGRI, and FALO. Surprisingly, BILT is found to have a poor correlation with NLST. This is somewhat unexpected since built-up areas are expected to be warmer during the night, and earlier studies, e.g., Pandey et al. 2014, have reported a significant positive correlation between LST and built-up areas over Delhi.

Further, low-lying areas are expected to be cooler during the night because of the temperature inversion, and hence, a positive (instead of negative) correlation is expected between NLST and ELEV. The negative correlation between NLST and ELEV has occurred due to the variable

behaviour of ELEV with NLST (i.e., first increasing and then decreasing with an increase in elevation). Figure 10 shows that a quadratic curve fits the scatter plot between NLST and ELEV reasonably well. To limit this effect, we performed correlation analysis of LST with percentage LULC and ELEV only for places in the study region that lie in the elevation range of 500 m to 700 m. These results are presented in Table 3. It is observed that now NLST has a significant positive correlation with ELEV and BILT.

Table 4 presents the results of multiple linear regression analysis for predicting DLST and NLST based on LULC and ELEV information for each grid cell. It is seen that ELEV has a significant negative regression coefficient while BILT, AGRI, and FALO have significant positive regression coefficients in the model for DLST. Further, these four variables together yield an R^2 value of more than 0.81 for explaining the variations in DLST. This indicates that

Fig. 9 Scatter plot between Aqua Night LST and Elevation



these four variables play a dominant role in determining the daytime variations of LST over the study region.

The model results for NLST (Table 4) show that ELEV, AGRI, and FALO remain significant variables during the nighttime also, but the nature of their relationship with NLST is different from that with DLST. The negative regression coefficients for AGRI and FALO indicate that these variables tend to reduce NLST. The relationship of ELEV with NLST is curvilinear (Fig. 10), and hence the night model contains a linear term (ELEV) and a quadratic term (ELEV²) to capture the relationship. The positive regression coefficient for ELEV suggests that at lower elevations, the positive linear association between NLST and ELEV will dominate. The negative regression coefficient of the ELEV² term indicates that at higher altitudes, the negative association dominates between NLST and ELEV. The fourth variable, i.e., BILT, is found to have a positive regression coefficient, but its p-value is slightly more than 0.05. Further, the R² values of 0.42 in the nighttime model suggest that though the LULC variables and ELEV play a significant role, their explanatory power is not as strong as it is during the day.

Implications of Warming on Cooling Degree Days and Energy Consumption

As UHIs have a substantial impact on a city's energy demand by elevating ambient temperatures, thereby increasing indoor space cooling requirements, Estimating the cooling degree days as an indicator of energy consumption due to space cooling, is a well established and accepted approach among the scientific community. Ukey and Rai (2021) clearly state that the degree days approach stands out due to its simplicity, transparency, and repeatability as indicators in predicting energy requirements for space cooling. One of the limitations in the present study is that we have not evaluated the impact of other variables such as relative humidity and wind speed which also impact energy consumption. However, Ukey and Rai (2021) further state that even though the degree days approach does not consider the effect of other variables like relative humidity and wind speed on energy consumption, they remain excellent indicators for explaining the variation in energy consumption. Similarly,

Fig. 9 (continued)

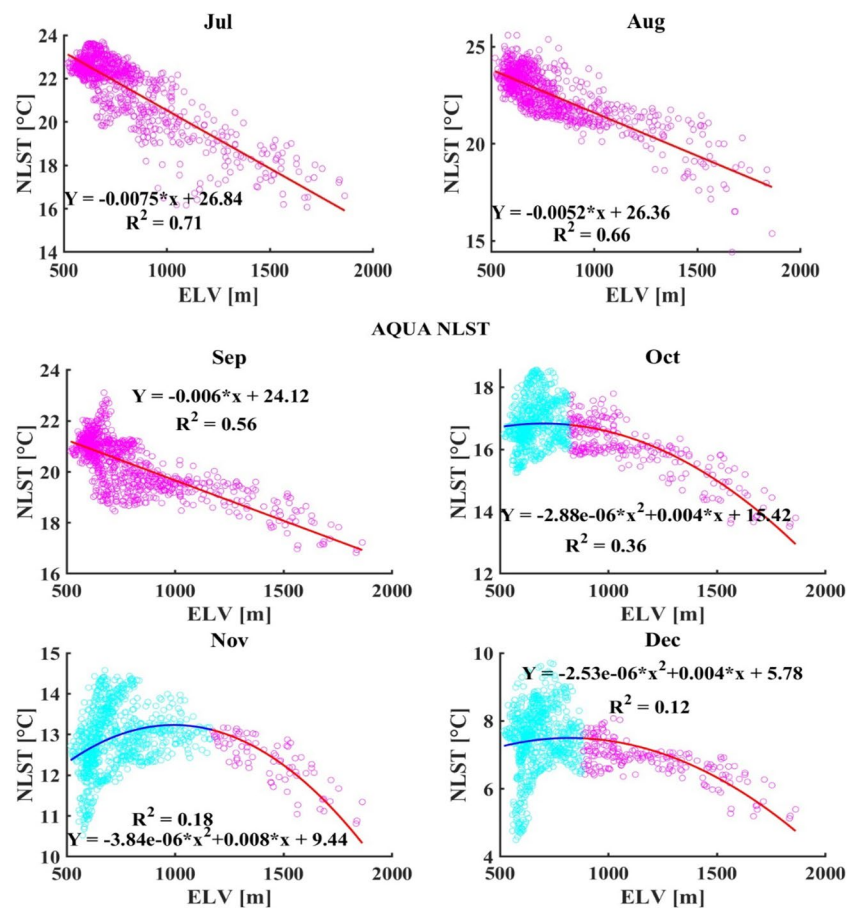


Table 2 Correlation matrix for the month of March (2019) at elevation (400–2000 m). (NLST-Night-time land surface temperature, DLST-Day time land surface temperature, ELEV-Elevation, DFOR-Dense Forest, OFOR-Open Forest, AGRI-Agriculture, FALO-Fallow land, BILT-Built up, WBOD-Water body, OPNS-Open space)

Variables	NLST	DLST	ELEV	DFOR	OFOR	AGRI	FALO	BILT	WBOD	OPNS
NLST	1	.140**	-.223**	.176**	0.026	-.304**	-.275**	0.03	-0.047	-0.06
DLST	.140**	1	-.790**	-.104*	-.655**	.416**	.210**	.615**	0.001	0.042
ELEV	-.223**	-.790**	1	-.159**	.668**	-.373**	-.295**	-.244**	-.168**	-.159**
DFOR	.176**	-.104*	-.159**	1	-.369**	-.317**	-.222**	-.410**	-.146**	-.148**
OFOR	0.026	-.655**	.668**	-.369**	1	-.369**	-.195**	-.458**	-.095*	-.126**
AGRI	-.304**	.416**	-.373**	-.317**	-.369**	1	.141**	.277**	-0.053	-0.067
FALO	-.275**	.210**	-.295**	-.222**	-.195**	.141**	1	-0.063	.326**	.414**
BILT	0.03	.615**	-.244**	-.410**	-.458**	.277**	-0.063	1	-.206**	-.167**
WBOD	-0.047	0.001	-.168**	-.146**	-.095*	-0.053	.326**	-.206**	1	.487**
OPNS	-0.06	0.042	-.159**	-.148**	-.126**	-0.067	.414**	-.167**	.487**	1

**Correlation is significant at the 0.01 level (2-tailed)

*Correlation is significant at the 0.05 level (2-tailed)

Rosa et al. 2015 also described degree days as a versatile climatic indicator for analysing energy consumption in a territory.

Figure 11 shows the trend in the annual magnitude and frequency of CDDs computed from (i) the daily mean air temperature data of the weather station over Dehradun (Fig. 11a and b) and (ii) daily mean air temperature of each pixel derived from LST (Fig. 11c and d). The increasing

trend in both the annual magnitude and frequency of CDDs is a noteworthy observation over Dehradun.

It is pertinent here to mention that the daily LST pixel data had missing values, and therefore, the trend values pertaining to weather station data and satellite-derived pixel data may not compare well. However, the trend values from the satellite-derived pixel data clearly show that the increasing trend is more pronounced over the places

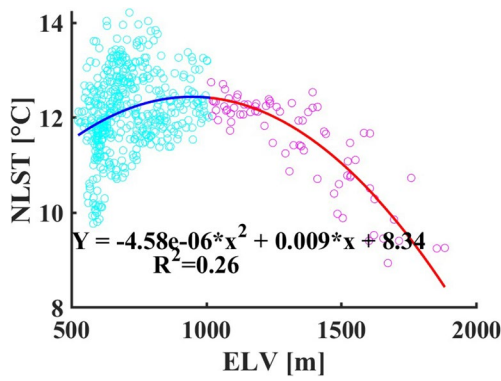


Fig. 10 Scatter plot between night-time LST and Elevation (ELEV)

which have witnessed the transformation of land-cover from agriculture/open forest to built-up. The increasing trend in CDDs suggests that electricity demand for cooling requirements of indoor spaces should have increased over Dehradun.

Figure 12 illustrates a noteworthy increase in the annual electricity consumption of Dehradun city. One may, however, attribute this increase to the rising trend in Dehradun’s population. However, when we compute the electricity consumption per capita, the increasing trend still persists (Fig. 12a). Thus, we observe that the increasing trend in the annual magnitude and frequency of CDDs over Dehradun is consistent with the increasing trend of per capita electricity consumption in the city.

Further, Fig. 12(b) shows a significant positive association between average annual air temperature and annual electricity consumption of Dehradun. This suggests that warming over Dehradun has been a contributing factor to the increasing trend of electricity consumption in the city.

Numerous studies (Garg et al. 2011; Rajagopalan et al. 2014; Li and Norford 2016; Ma et al. 2018) indicate that the implementation of UHI mitigation techniques, e.g., cool roofs, vertical gardens, high albedo surfaces, and increased greenery in urban areas, could potentially lead to a reduction in ambient air temperatures by 3 °C to 4 °C. In the light of the fact that Dehradun

Table 3 Correlation matrix for the month of March (2019) at Elevation (500-700 m). (NLST-Night-time land surface temperature, DLST-Day time land surface temperature, ELEV-Elevation, DFOR-Dense Forest, OFOR-Open Forest, AGRI-Agriculture, FALO-Fallow land, BILT-Built up, WBOD-Water body, OPNS-Open space)

Variables	NLST	DLST	ELEV	DFOR	OFOR	AGRI	FALO	BILT	WBOD	OPNS
NLST	1	0.054	.327**	0.089	.137*	-.385**	-.393**	.201**	-0.117	-0.077
DLST	0.054	1	-0.001	-.569**	-.278**	.237**	-0.09	.775**	-.181**	-.157*
ELEV	.327**	-0.001	1	.368**	-0.015	-.404**	-.179**	0.049	-.270**	-.168**
DFOR	0.089	-.569**	.368**	1	-0.114	-.439**	-.290**	-.522**	-.148*	-.167**
OFOR	.137*	-.278**	-0.015	-0.114	1	-.202**	0.048	-.418**	-0.079	-0.073
AGRI	-.385**	.237**	-.404**	-.439**	-.202**	1	-0.003	.134*	-.154*	-.175**
FALO	-.393**	-0.09	-.179**	-.290**	0.048	-0.003	1	-.261**	.352**	.442**
BILT	.201**	.775**	0.049	-.522**	-.418**	.134*	-.261**	1	-.289**	-.279**
WBOD	-0.117	-.181**	-.270**	-.148*	-0.079	-.154*	.352**	-.289**	1	.503**
OPNS	-0.077	-.157*	-.168**	-.167**	-0.073	-.175**	.442**	-.279**	.503**	1

**Correlation is significant at the 0.01 level (2-tailed)

*Correlation is significant at the 0.05 level (2-tailed)

Table 4 Results of Regression analysis for the month of March (2019) at elevation (400-2000 m)

Model description	Dependent Variables	Explanatory Variables	B	Std. error	t value	Sig Value	R ²
Regression model for March-Day time	DLST	(Constant)	303.325	0.189	1601.3	0.00	0.81
		ELEV	-0.006	0	-30.7	0.00	
		AGRI	0.008	0.004	2.1	0.04	
		FALO	0.013	0.007	2.0	0.05	
		BILT	0.042	0.002	22.4	0.00	
Regression model for March-Night-time	NLST	(Constant)	283.661	0.399	711.8	0.00	0.42
		ELEV ²	-3.23 × 10 ⁻⁰⁶	0	-8.9	0.00	
		ELEV	0.005	0.001	6.6	0.00	
		AGRI	-0.023	0.003	-8.8	0.00	
		FALO	-0.041	0.005	-8.6	0.00	
		BILT	0.002	0.001	1.8	0.07	

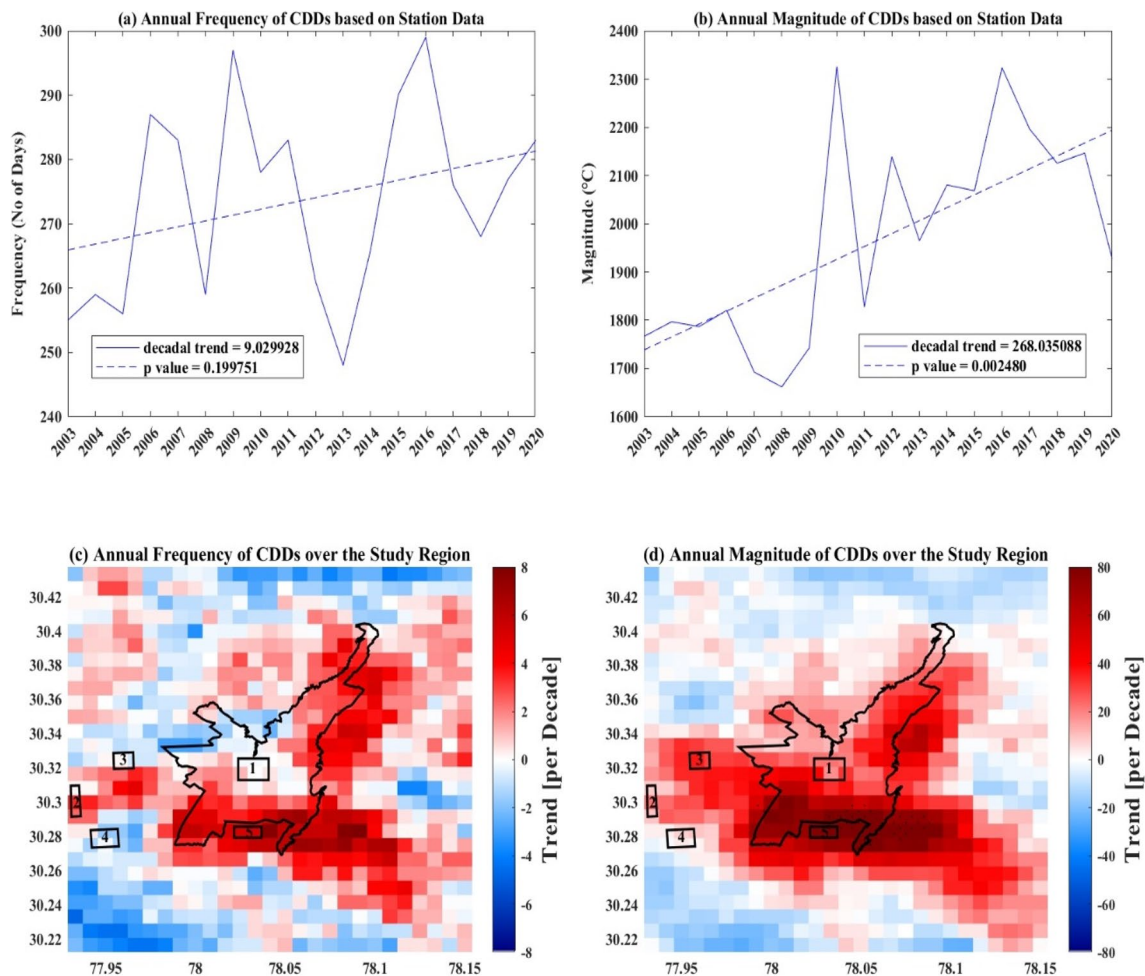


Fig. 11 (a) Scatter plot between annual magnitude of cooling degree days (CDD) over years, (b) Scatter plot between frequency of cooling degree days (CDD) over years. (c) Trend in annual frequency of CDDs, (d) Trend in annual magnitude of CDDs

is part of the smart city mission launched by the Indian Government, the adoption of appropriate UHI mitigation measures is very much required for the city of Dehradun. Even a reduction of 1 °C in the average air temperature of Dehradun should lead to substantial electricity consumption savings for the city.

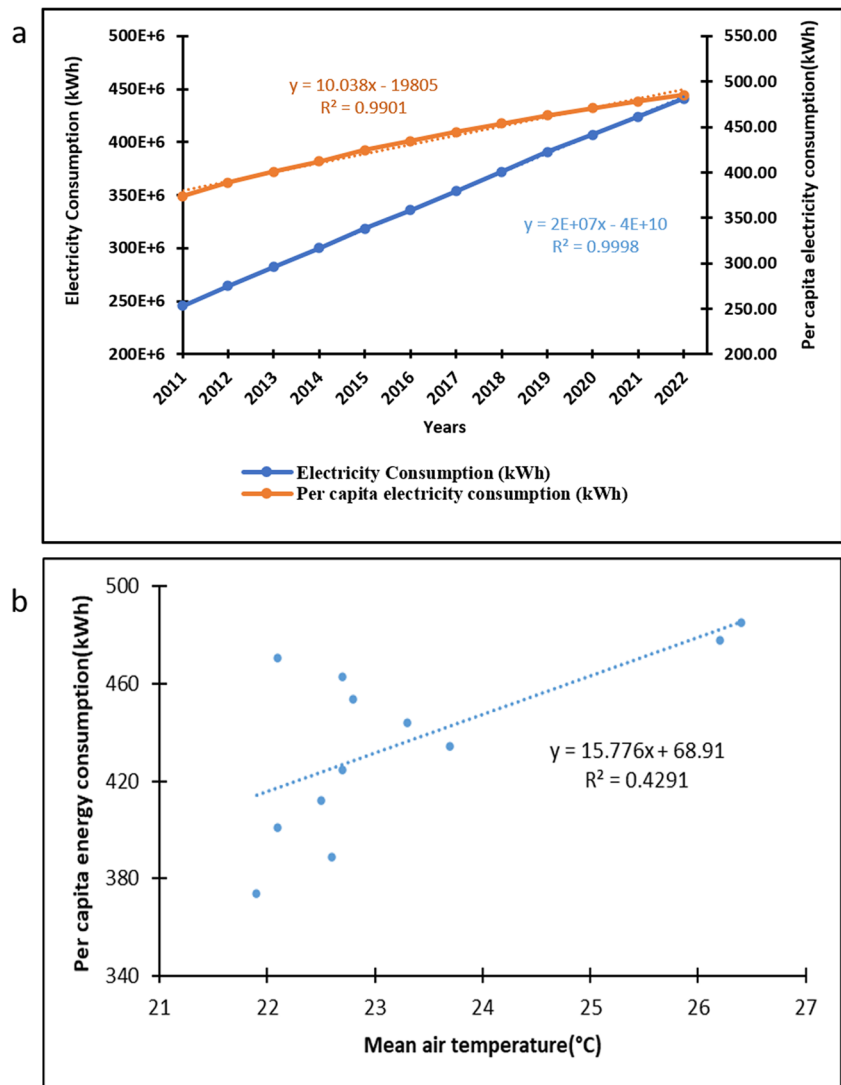
Conclusion

Our study shows that Dehradun city and its adjoining surrounding areas, particularly in the southern and eastern regions, have witnessed urbanization over the last two decades. The Land Surface Temperature (LST) trends over the study region indicate that areas undergoing a transition in Land Use and Land Cover (LULC) from agriculture/open forest to built-up have experienced the greatest increase in LST. We have also observed diurnal asymmetry in LST trends over the study region, which is best explained by the increase in cloud cover under the global warming effect.

Furthermore, the Urban Heat Island (UHI) formation over Dehradun persists throughout the year. However, the magnitude of UHI during the daytime (~2–6 °C for Terra and ~4–9 °C for Aqua) is generally greater than that during the night-time (~1.5–3.5 °C for Terra and ~0.5–2 °C for Aqua), possibly because the thermal inertia of the surrounding vegetated area is greater than that of the built-up area. Additionally, the magnitude of Surface Urban Heat Island Intensity (SUHII) is found to be maximum during the rainy season (>6 °C) and minimum during winter (<2 °C) as the thermal inertia of the surrounding wet soil covered with vegetation is even higher during the wet period compared to the dry winter.

Our correlation and regression results indicate that Elevation (ELEV), along with LULC variables such as Agriculture (AGRI), Fallow Land (FALO), and Built-Up (BILT), significantly affects the LST of a place in the study area. Moreover, ELEV is found to have a negative relationship with LST during the daytime. However, at

Fig. 12 (a-b) Scatter plots between (a) Annual electricity consumption with per capita electricity consumption over the years, (b) Per capita electricity consumption and mean air temperature



night, the relationship between ELEV and LST becomes curvilinear due to the effect of the local slope factor, allowing cold air to settle at lower altitudes of up to 1000 m. Thus, night-time LST is found to increase with elevation up to 1000 m, and thereafter, LST decreases with elevation as it does during the daytime.

There is also an increasing trend in the annual magnitude as well as the annual frequency of Cooling Degree Days (CDDs) over Dehradun city. However, the trend values from satellite-based pixel data clearly show the increasing trend is more prominent over areas showing a transformation of land-cover from agriculture/open forest to built-up. The rising trend in CDDs also indicates that electricity demand for cooling requirements of indoor spaces is likely to have increased over Dehradun city.

In summary, our study reveals warming trends over Dehradun city due to the combined effect of the Urban Heat Island and global warming. This warming is

particularly pronounced over areas that have undergone urbanization. These changes in the thermal climate of the city have led to increased energy consumption to improve human comfort levels, providing a positive feedback loop. In other words, urbanization in Dehradun has led to increased warming, which in turn, has resulted in increased energy consumption, releasing anthropogenic heat in the process, which further contributes to warming. Given that Dehradun city falls under the ambit of the 'Indian Government Smart Cities Mission,' it is necessary to establish a conceptual framework for future urban planning to achieve the mission goals. This may involve developing regulations that promote the increase in green spaces, cool rooftops, pervious surfaces, water bodies, and green buildings in the city to mitigate urban heating. In this regard, our study offers useful insights for urban policymakers, especially in the context of cities with hilly terrain.

Supplementary Information The online version contains supplementary material available at <https://doi.org/10.1007/s41651-024-00178-0>.

Acknowledgements The authors are thankful to acknowledge School of Environmental Sciences (SES), Jawaharlal Nehru University for providing necessary facilities to conduct this study. Authors wish their thanks to Moderate Resolution Imaging Spectroradiometer (MODIS), LANDSAT-7, SENTINEL-2 and ASTER scientific and data support teams, which are maintained to provide data freely. Authors also acknowledge the University Grant Commission of India for providing financial support to research scholars involved in this study.

Funding This research did not receive any specific grant from funding agencies in the public, commercial, or not-for-profit sectors.

Data Availability The data used in this article are sourced exclusively from open-access repositories. All data outputs generated during the study are publicly available and are properly cited in this paper.

Declarations

Ethics Approval The methodologies, findings, and conclusions presented here are derived from original research work according to our knowledge and opinion.

Informed Consent All the co-authors are kept informed during every step of publication processes and all processing is done by their consent.

Conflict of Interest The authors declare no competing interests.

References

- Air temperature data (n.d.). <https://www.visualcrossing.com/>. Accessed 10 Sept 2023
- Akbari H, Pomerantz M, Taha H (2001) Cool surfaces and shade trees to reduce energy use and improve air quality in urban areas. *Sol Energy* 70(3):295–310
- Arnfield AJ (1982) Estimation of diffuse irradiance on sloping, obstructed surfaces: An error analysis. *Archiv Meteorol, Geophysics, and Bioclimatology Series B* 30(4):303–320. <https://doi.org/10.1007/BF02324672>
- Ball F (1956) The Theory of Strong Katabatic Winds. *Aust J Phys* 9(3):373. <https://doi.org/10.1071/ph560373>
- Bhatnagar M, Mathur J, Garg V (2018) Determining base temperature for heating and cooling degree-days for India. *J Build Eng* 18:270–280
- Borah P, Singh MK, Mahapatra S (2015) Estimation of degree-days for different climatic zones of North-East India. *Sustain Cities Soc* 14:70–81
- Buyantuyev A, Wu J (2010) Urban heat islands and landscape heterogeneity: linking spatiotemporal variations in surface temperatures to land-cover and socioeconomic patterns. *Landsc Ecol* 25:17–33
- Carnahan WH, Larson RC (1990) An Analysis of an Urban Heat Sink. *Remote Sens Environ* 33(1):65–71. [https://doi.org/10.1016/0034-4257\(90\)90056-R](https://doi.org/10.1016/0034-4257(90)90056-R)
- Chakraborty T, Hsu A, Manya D, Sheriff G (2020) A spatially explicit surface urban heat island database for the United States: Characterization, uncertainties, and possible applications. *ISPRS J Photogramm Remote Sens* 168:74–88
- Chetry V (2022) Geospatial measurement of urban sprawl using multi-temporal datasets from 1991 to 2021: case studies of four Indian medium-sized cities. *Environ Monit Assess* 194(12):860
- Chetry V (2023) A Critical Review of Urban Sprawl Studies. *J Geovis Spat Anal* 7:28. <https://doi.org/10.1007/s41651-023-00158-w>
- Christenson M, Manz H, Gyalistras D (2006) Climate warming impact on degree-days and building energy demand in Switzerland. *Energy Convers Manage* 47(6):671–686
- Cox DTC, Maclean IMD, Gardner AS, Gaston KJ (2020) Global variation in diurnal asymmetry in temperature, cloud cover, specific humidity and precipitation and its association with leaf area index. *Glob Change Biol* 26(12):7099–7111. <https://doi.org/10.1111/gcb.15336>
- Dame J, Schmidt S, Müller J, Nüsser M (2019) Urbanisation and socio-ecological challenges in high mountain towns: Insights from Leh (Ladakh), India. *Landsc Urban Plan* 189:189–199
- De Rosa M, Bianco V, Scarpa F, Tagliafico LA (2015) Historical trends and current state of heating and cooling degree days in Italy. *Energy Convers Manage* 90:323–335
- Dehradun Population (n.d.). <https://www.census2011.co.in/census/district/578-dehradun.html>. Accessed 23 May 2023
- Diksha KA, Lal P (2022) Analysing climatic variability and extremes events in the Himalayan regions focusing on mountainous urban agglomerations. *Geocarto Int* 37(26):14148–14170
- Dutta K, Basu D, Agrawal S (2022) Evaluation of seasonal variability in magnitude of urban heat islands using local climate zone classification and surface albedo. *Int J Environ Sci Technol* 19(9):8677–8698. <https://doi.org/10.1007/s13762-021-03602-w>
- Estoque RC, Murayama Y (2017) Monitoring surface urban heat island formation in a tropical mountain city using Landsat data (1987–2015). *ISPRS J Photogramm Remote Sens* 133:18–29. <https://doi.org/10.1016/j.isprsjprs.2017.09.008>
- Ganasri BP, Dwarakish GS (2015) Study of land use/land cover dynamics through classification algorithms for Harangi catchment area, Karnataka State, India. *Aquatic Procedia* 4:1413–1420
- Garg V, Chandrasen K, Mathur J, Tetali S, Jawa A (2011) Development and performance evaluation of a methodology, based on distributed computing, for speeding energyplus simulation. *J Build Perform Simul* 4(3):257–270. <https://doi.org/10.1080/19401493.2010.531142>
- Goward SN, Masek JG, Williams DL, Irons JR, Thompson RJ (2001) The Landsat 7 mission: Terrestrial research and applications for the 21st century. *Remote Sens Environ* 78(1–2):3–12. [https://doi.org/10.1016/S0034-4257\(01\)00262-0](https://doi.org/10.1016/S0034-4257(01)00262-0)
- Gu RY, Lo MH, Liao CY, Jang YS, Juang JY, Huang CY, Chang SC, Hsieh CI, Chen YY, Chu H, Chang KY (2021) Early Peak of Latent Heat Fluxes Regulates Diurnal Temperature Range in Montane Cloud Forests. *J Hydrometeorol* 22(9):2475–2487. <https://doi.org/10.1175/JHM-D-21-0005.1>
- Habeeb R, Gupta Y, Chinwan H et al (2019) Assessing Demographic and Water Sensitivities Arising due to Urban Water Insecurity in Haldwani, Uttarakhand (India): a GIS-Based Spatial Analysis. *J Geovis Spat Anal* 3:8. <https://doi.org/10.1007/s41651-019-0031-4>
- Hansen J, Sato M (2004) Greenhouse gas growth rates. *Proc Natl Acad Sci* 101(46):16109–16114
- Hawkins E, Ortega P, Suckling E, Schurer A, Hegerl G, Jones P, ..., Van Oldenborgh GJ (2017) Estimating changes in global temperature since the preindustrial period. *Bull Am Meteorol Soc* 98(9):1841–1856
- Hirano A, Welch R, Lang H (2003) Mapping from ASTER stereo image data: DEM validation and accuracy assessment. *ISPRS J Photogramm Remote Sens* 57(5–6):356–370. [https://doi.org/10.1016/S0924-2716\(02\)00164-8](https://doi.org/10.1016/S0924-2716(02)00164-8)
- Hishe H, Giday K, Van Orshoven J, Muys B, Taheri F., Azadi H, ..., Witlox F (2021) Analysis of land use land cover dynamics and driving factors in Desa’a forest in Northern Ethiopia *Land use policy* 101 105039
- Jiang F, Li X, Wei B, Hu R, Li Z (2009) Observed trends of heating and cooling degree-days in Xinjiang Province, China. *Theoret Appl Climatol* 97:349–360

- Joshi N (2021) Adopting a governance lens to address urban risks in the Uttarakhand Himalayas: The case of Almora India. *Int J Disaster Risk Reduct* 54:102044. <https://doi.org/10.1016/j.ijdrr.2021.102044>
- Khandelwal S, Goyal R, Kaul N, Mathew A (2018) Assessment of land surface temperature variation due to change in elevation of area surrounding Jaipur, India. *Egyptian Journal of Remote Sensing and Space Science* 21(1):87–94. <https://doi.org/10.1016/j.ejrs.2017.01.005>
- Kimothi S, Thapliyal A, Gehlot A, Aledaily AN, Bilandi N, Singh R, ..., Akram SV (2023) Spatio-temporal fluctuations analysis of land surface temperature (LST) using Remote Sensing data (LANDSAT TM5/8) and multifractal technique to characterize the urban heat Islands (UHIs). *Sustain Energy Technol Assessments* 55:102956
- Kumari P, Garg V, Kumar R, Kumar K (2021) Impact of urban heat island formation on energy consumption in Delhi. *Urban Climate* 36(January):100763. <https://doi.org/10.1016/j.uclim.2020.100763>
- Landsat-7 data (n.d.) <https://www.usgs.gov/landsat-missions/landsat-7>. Accessed on 15 March 2019
- Li XX, Norford LK (2016) Evaluation of cool roof and vegetations in mitigating urban heat island in a tropical city, Singapore. *Urban Climate* 16:59–74. <https://doi.org/10.1016/j.uclim.2015.12.002>
- Li X, Zhou Y, Asrar GR, Imhoff M, Li X (2017) The surface urban heat island response to urban expansion: A panel analysis for the conterminous United States. *Sci Total Environ* 605:426–435
- Liao D, Zhu H, Jiang P (2021) Study of urban heat island index methods for urban agglomerations (hilly terrain) in Chongqing. *Theoret Appl Climatol* 143(1–2):279–289. <https://doi.org/10.1007/s00704-020-03433-8>
- Lu S, Ju Z, Ren T, Horton R (2009) A general approach to estimate soil water content from thermal inertia. *Agric for Meteorol* 149(10):1693–1698. <https://doi.org/10.1016/j.agrformet.2009.05.011>
- Ma S, Pitman A, Yang J, Carouge C, Evans JP, Hart M, Green D (2018) Evaluating the effectiveness of mitigation options on heat stress for Sydney, Australia. *J Appl Meteorol Climatol* 57(2):209–220. <https://doi.org/10.1175/JAMC-D-17-0061.1>
- Mishra PK, Rai A, Rai SC (2020) Land use and land cover change detection using geospatial techniques in the Sikkim Himalaya, India. *Egypt J Remote Sens Space Sci* 23(2):133–143
- Mohajerani A, Bakaric J, Jeffrey-Bailey T (2017) The urban heat island effect, its causes, and mitigation, with reference to the thermal properties of asphalt concrete. *J Environ Manage* 197:522–538
- Morshed M, Chakraborty T, Mazumder T (2022) Measuring Dhaka's Urban Transformation Using Nighttime Light Data. *J Geovis Spat Anal* 6:25. <https://doi.org/10.1007/s41651-022-00120-2>
- Oke TR (1981) Canyon Geometry and the Nocturnal Urban Heat Island: Comparison of Scale Model and Field Observations. *J Climatol* 1:237–254. <https://doi.org/10.1002/joc.3370010304>
- Oke TR (1982) The energetic basis of the urban heat island. *Q J R Meteorol Soc* 108(455):1–24. <https://doi.org/10.1002/qj.49710845502>
- Oke TR, Mills G, Christen A, Voogt JA (2017) *Urban climates*. Cambridge University Press
- Oke, T. R. (2010). *Urban heat islands*. In *The Routledge Handbook of urban ecology* (pp. 120–131). Routledge
- Otukei JR, Blaschke, T (2010) Land cover change assessment using decision trees, support vector machines and maximum likelihood classification algorithms. *Int J Appl Earth Obs Geoinf*, 27–31. <https://doi.org/10.1016/j.jag.2009.11.002>
- Pandey P, Kumar D, Prakash A, Masih J, Singh M, Kumar S, Jain VK, Kumar K (2012) A study of urban heat island and its association with particulate matter during winter months over Delhi. *Sci Total Environ* 414:494–507. <https://doi.org/10.1016/j.scitotenv.2011.10.043>
- Pandey AK, Singh S, Berwal S, Kumar D, Pandey P, Prakash A, Lodhi N, Maithani S, Jain VK, Kumar K (2014) Spatio-temporal variations of urban heat island over Delhi. *Urban Climate* 10(P1):119–133. <https://doi.org/10.1016/j.uclim.2014.10.005>
- Papadopoulos KH, Helmis CG (1999) Evening and morning transition of katabatic flows. *Boundary-Layer Meteorology* 92:195–227
- Phiri D, Simwanda M, Salekin S, Ryirenda VR, Murayama Y, Ranagalage M, Oktaviani N, Kusuma HA, Zhang T, Su J, Liu C, Chen WH, Liu H, Liu G, Cavour M, Duzgun HS, Kemec S, Demirkan DC, Chairer R, ..., Peerbhay K (2020) Sentinel-2 Data for Land Cover / Use Mapping : A Review. *Remote Sens* 42(3):14. <https://doi.org/10.3390/rs12142291>
- Priyadarsini R (2009) Urban heat island and its impact on building energy consumption. *Adv Build Energy Res* 3(1):261–270
- Pu R, Gong P, Michishita R, Sasagawa T (2006) Assessment of multi-resolution and multi-sensor data for urban surface temperature retrieval. *Remote Sens Environ* 104(2):211–225
- Pyrgou A, Santamouris M, Livada I (2019) Spatiotemporal analysis of diurnal temperature range: Effect of urbanization, cloud cover, solar radiation, and precipitation. *Climate* 7(7):1–13. <https://doi.org/10.3390/cli7070089>
- Rajagopalan P, Lim KC, Jamei E (2014) Urban heat island and wind flow characteristics of a tropical city. *Sol Energy* 107:159–170. <https://doi.org/10.1016/j.solener.2014.05.042>
- Rana VK, Suryanarayana TMV (2019) Visual and statistical comparison of ASTER, SRTM, and Cartosat digital elevation models for watershed. *J Geovis Spat Anal* 3:12. <https://doi.org/10.1007/s41651-019-0036-z>
- Rieck M, Hohenegger C, van Heerwaarden CC (2014) The influence of land surface heterogeneities on cloud size development. *Mon Weather Rev* 142(10):3830–3846. <https://doi.org/10.1175/MWR-D-13-00354.1>
- Romshoo SA, Rashid I (2014) Assessing the impacts of changing land cover and climate on Hokersar wetland in Indian Himalayas. *Arab J Geosci* 7:143–160
- Rongali G, Keshari AK, Gosain AK et al (2018) Split-Window Algorithm for Retrieval of Land Surface Temperature Using Landsat 8 Thermal Infrared Data. *J Geovis Spat Anal* 2:14. <https://doi.org/10.1007/s41651-018-0021-y>
- Saha S, Saha A, Das M, Saha A, Sarkar R, Das A (2021) Analyzing spatial relationship between land use/land cover (LULC) and land surface temperature (LST) of three urban agglomerations (UAs) of Eastern India. *Remote Sens Appl Soc Environ* 22:100507
- Schurer AP, Mann ME, Hawkins E, Tett SF, Hegerl GC (2017) Importance of the pre-industrial baseline for likelihood of exceeding Paris goals. *Nat Clim Chang* 7(8):563–567
- Sharma A, Singh OP, Saklani MM (2012) *Climate of Dehradun*. Indian Meteorological Department, Government of India, Ministry of Earth Sciences, Mausam Bhavan, New Delhi, 69
- Shastri H, Barik B, Ghosh S, Venkataraman C, Sadavarte P (2017) Flip flop of Day-night and Summer-Winter Surface Urban Heat Island Intensity in India. *Sci Rep* 7:1–8. <https://doi.org/10.1038/srep40178>
- Singh A, Pal S, Kanungo DP (2021) An integrated approach for landslide susceptibility–vulnerability–risk assessment of building infrastructures in hilly regions of India. *Environ Dev Sustain* 23(4):5058–5095
- Sobrino JA, El Kharraz MH (1999) Combining afternoon and morning NOAA satellites for thermal inertia estimation 1 Algorithm and its testing with Hydrologic Atmospheric Pilot Experiment-Sahel data. *J Geophys Res Atmos* 104(D8):9445–9453 <https://doi.org/10.1029/1998JD200109>

- Sobrino JA, Oltra-Carrió R, Sòria G, Jiménez-Muñoz JC, Franch B, Hidalgo V, ..., Paganini M (2013) Evaluation of the surface urban heat island effect in the city of Madrid by thermal remote sensing. *Int J Remote Sens* 34(9–10):3177–3192
- Strahler AH (1980) The use of prior probabilities in maximum likelihood classification of remotely sensed data. *Remote Sens Environ* 10(2):135–163. [https://doi.org/10.1016/0034-4257\(80\)90011-5](https://doi.org/10.1016/0034-4257(80)90011-5)
- Sun J, Yang J, Zhang C, Yun W, Qu J (2013) Automatic remotely sensed image classification in a grid environment based on the maximum likelihood method. *Math Comput Model* 58(3–4):573–581
- Tabassum A, Basak R, Shao W, Haque MM, Chowdhury TA, Dey H (2023) Exploring the relationship between land use land cover and land surface temperature: a case study in Bangladesh and the policy implications for the Global South. *J Geovisualization Spat Anal* 7(2):25
- Taha H (1997) Urban climates and heat islands: albedo, evapotranspiration, and anthropogenic heat. *Energy Build* 25(2):99–103
- Ukey R, Rai AC (2021) Impact of global warming on heating and cooling degree days in major Indian cities. *Energy Build* 244:111050
- Ullah S, Ahmad K, Sajjad RU, Abbasi AM, Nazeer A, Tahir AA (2019) Analysis and simulation of land cover changes and their impacts on land surface temperature in a lower Himalayan region. *J Environ Manage* 245:348–357
- Vancutsem C, Ceccato P, Dinku T, Connor SJ (2010) Evaluation of MODIS land surface temperature data to estimate air temperature in different ecosystems over Africa. *Remote Sens Environ* 114(2):449–465
- Vihma T, Tuovinen E, Savijrvi H (2011) Interaction of katabatic winds and near-surface temperatures in the Antarctic. *J. Geophys Res Atmos* 116(21):1–14. <https://doi.org/10.1029/2010JD014917>
- Voogt JA, Oke TR (2003) Thermal remote sensing of urban climates. *Remote Sens Environ* 86(3):370–384. [https://doi.org/10.1016/S0034-4257\(03\)00079-8](https://doi.org/10.1016/S0034-4257(03)00079-8)
- Wan Z, Zhang Y, Zhang Q, Li ZL (2002) Validation of the land-surface temperature products retrieved from terra moderate resolution imaging spectroradiometer data. *Remote Sens Environ* 83(1–2):163–180. [https://doi.org/10.1016/S0034-4257\(02\)00093-7](https://doi.org/10.1016/S0034-4257(02)00093-7)
- Weng Q, Fu P, Gao F (2014) Generating daily land surface temperature at Landsat resolution by fusing Landsat and MODIS data. *Remote Sens Environ* 145:55–67
- World Urbanization Prospects (2018) <https://population.un.org/wup/>. Accessed 15 Sept 2022
- Yuan F, Sawaya KE, Loeffelholz BC, Bauer ME (2005) Land cover classification and change analysis of the Twin Cities (Minnesota) metropolitan area by multitemporal Landsat remote sensing. *Remote Sens Environ* 98(2–3):317–328. <https://doi.org/10.1016/j.rse.2005.08.006>

Publisher's Note Springer Nature remains neutral with regard to jurisdictional claims in published maps and institutional affiliations.

Springer Nature or its licensor (e.g. a society or other partner) holds exclusive rights to this article under a publishing agreement with the author(s) or other rightsholder(s); author self-archiving of the accepted manuscript version of this article is solely governed by the terms of such publishing agreement and applicable law.